

Understanding divertor detachment  
through CRETIN modeling —  
a work in progress

M.L. Adams<sup>1</sup>, X. Bonnin, J.L. Terry,  
A.Yu. Pigarov<sup>2,3</sup>, H.A. Scott<sup>4</sup>  
and S.I. Krasheninnikov<sup>2</sup>

September 1998

<sup>1</sup>e-mail: adams@mit.edu

<sup>2</sup>Also at I.V. Kurchatov Institute of Atomic Energy, Moscow, Russian Federation

<sup>3</sup>Also at College of William and Mary, Williamsburg, VA

<sup>4</sup>Lawrence Livermore National Laboratory, P.O. Box 808, L-18, Livermore, CA 94550, USA

# 1 Introduction

From numerous studies aimed at reducing the divertor target plate incident heat flux or understanding divertor detachment, an abundance of evidence supporting the importance of atomic processes in tokamak plasmas now exists. Through use of a multi-dimensional Non-Local Thermodynamic Equilibrium (NLTE) simulation code named CRETIN [1] this report seeks to quantify some of this evidence and highlight important areas for future research.

Throughout the history of plasma physics, researchers have been attune to the presence of atoms, molecules and atomic ions in their excited states. A seemingly periodic trend in the level of emphasis placed on the importance of atomic processes is approaching another peak, bringing about a new push toward including atomic processes in current theoretical and computational models. A previous peak, beginning in the late 70's, involved the use of models based on the assumption of Coronal Equilibrium (CE) to investigate impurity removal *from* the central plasma.[2, 3, 4] Ironically, in the early 90's researchers used the same models to study impurity puffing *into* the central plasma, creating a “radiative mantle”. Today, an interest in atomic processes began again when both theory and computer simulations indicated that within the divertor region recombination rates may best be explained through Collisional Radiative (CR) theory.[5, 6] Subsequent experiments carried out in Alcator C-Mod have verified such predictions [7] and efforts are now being made to apply CR theory, *via* computer simulation (CRETIN), to further our understanding divertor detachment and known related phenomenon (for example, MARFE's).

To some, there is still a question of why CE models are unable to describe all atomic phenomenon occurring within tokamaks — they worked in the past so why not continue their use? CE theory is valid for high-temperature low-density plasmas, such as those encountered within the separatrix of tokamak reactors in normal modes of operation, and does not offer reasonable results for tokamak regions within the divertor where temperatures may be below 1 eV and densities above  $10^{14} \text{ cm}^{-3}$ . These regions are best characterized by use of a Collisional Radiative (CR) model. To further highlight their differences we contrast collisional time scales. Excited atoms characterized by CR theory will tend to transfer excess energy through collisional processes; when characterized by CE theory, excited atoms are more likely to radiate their excess energy and drop to the ground state. Whereas a simple balance between electron ionization and recombination would suffice in CE models, a tokamak plasma within a CR regime must self-consistently account for both photons, or the radiation field, and neutrals. Thus, codes based on CR theory look to solve a system of atomic rate equations, the radiation transfer equation, and traditional transport equations describing neutrals and plasmas.

This report is divided as follows: *Section 2* covers CRETIN’s transition from an Inertial Confinement Fusion (ICF) tool to a code useful for tokamak simulations; *Section 3* seeks to quantify the importance of opacity on critical diagnostic lines; *Section 4* presents initial Alcator C-Mod 1-D midplane MARFE simulation results; and *Section 5* is composed of recommendations for evolving CRETIN toward a code capable of modeling divertor detachment. The reader will note that an abstract and conclusion section have been omitted; this report is meant for discussion purposes.

## 2 CRETIN Modifications

CRETIN is a multi-dimensional Non-Local Thermodynamic Equilibrium (NLTE) simulation code originally developed based on the high-temperature low-density “isolated atom” treatment of atomic kinetics. It was then adapted for Inertial Confinement Fusion (ICF) conditions where efforts were made to use physics elements appropriate for higher densities. Use in divertor simulations has required some ICF dependent aspects of CRETIN to be altered.

### 2.1 New Excitation and Ionization Cross-Section Fits

CRETIN’s original hydrogen atomic model used excitation and ionization cross-section fits valid in the temperature range  $300 < T \text{ eV} < 1000$ , well above divertor operating conditions. Rather than extrapolate the original fits, a process which was found to be unreliable, a new set of fits were devised. Using data from tables published by Johnson and Hinnov [8, 9], cross-section fits relevant to the temperature range  $0.3 < T \text{ eV} < 100$  were constructed.

### 2.2 New Hydrogen Line Stark Width Fits

Similar to the cross-section fits, the line Stark width fits were not valid for hydrogen plasmas. CRETIN used fits by Lee [10] for the  $Ly_{\beta,\delta}$  lines and an empirical formula by Griem for all other lines. All hydrogen line Stark width fits have been replaced by interpolation of other Griem calculations more suitable to low-temperature medium-density regimes, but still neglecting ion dynamics effects.[11] Although Livermore is currently working to provide fits that can be applied over a wide range of conditions, at this time no attempt has been made to resolve the individual Stark components and only a Lorentzian half-width is computed.

## 2.3 New Rate Matrix Solution Technique

In our initial simulations it was necessary to independently impose electron and atom density profiles, in contrast to just using the total density. This has been implemented through the definition of a new switch whose features we highlighted in this subsection. Before beginning, a few parameters will be defined:

$n_e$	electron density
$n_a$	$\left\{ \begin{array}{l} H^+ \text{ ions whose density is } n_+, \\ H_0 \text{ ground state} \\ H^* \text{ and all excited states } (n = 2, \dots, 10) \end{array} \right.$
$n_g$	ground state density
$n_k$	density of excited state with principal quantum number $n = k$
$n_0$	neutral density ( $n_0 = n_g + \sum_k n_k$ )

A simple radiation transfer benchmark problem is the steady-state, spatially homogeneous plasma when only  $T_e$  and one atomic state density are necessary to obtain a unique solution. In addition, if another constraint is needed, such as two atomic state densities instead of one, the atomic rate matrix must be modified. For divertor studies it was necessary to independently impose  $n_e$  (and hence  $n_+$  through quasi-neutrality) as well as  $n_a$ .

Before any alterations, the atomic rate equations have the form:

$$A \cdot N = B,$$

where  $N$  denotes a vector whose components span the range of occupation numbers,  $A$  is an  $(N \times N)$  rate matrix containing relevant CR atomic processes and radiative transfer effects, and  $B$  is a vector containing the time derivatives of the population densities. When imposing  $n_+$ , the corresponding row in  $A$  is replaced as follows:

$$\begin{aligned} A_{+i} &= 0 \quad \forall (i \neq +) \\ A_{++} &= 1 \\ B_+ &= n_e \quad , \end{aligned}$$

where  $+$  is the index of the  $H^+$  state. If a subsequent constraint is placed upon  $n_0$ , then  $A$  is modified as follows:

$$\begin{aligned} A_{gg} &= 1 \\ A_{gk} &= 1 \quad \forall k \\ A_{g+} &= 0 \\ B_g &= n_0 \quad , \end{aligned}$$

where  $g$  is the index of the ground  $H_0$  state.

When solving the above linear system of equations in 1-D, CRETIN makes only one pass. Since our benchmark problems were over-constrained, it is possible for the solution to yield non-physical densities. For example, since the code does not check whether  $n_a$  is larger than  $n_e$  (both being user defined quantities) negative densities may result. Also, if the temperature is low enough for recombination to heavily populate the excited states, reduced ground state populations are possible and negative populations will result since the latter is given by  $n_g = n_0 - \sum_k n_k$ . Abnormalities such as these will not be corrected through the evolution of the solution in time, and the user must be careful.

### 3 Opacity Importance in a Simple Plasma Problem

Sensitivity of the ionization balance to the plasma parameters which determine it —  $T_e$ ,  $n_e$ , and opacity of the partially ionized plasma to the D<sup>0</sup> Lyman lines — is shown in Fig. 1 for cases with no particle transport. At low densities ( $n_e + N^0 = 10^{16} \text{ m}^{-3}$ , shown by the dot-dashed curves) single-step ionization competes against radiative recombination. The dashed curves illustrate the case at divertor-like densities ( $n_e + N^0 = 10^{21} \text{ m}^{-3}$ ), but where the effects of radiation transfer are neglected (therefore a non-physical case). Since the increased 3-body recombination occurring at the higher density is outweighed by the increase in multi-step ionization, the temperature at which  $n_e = N^0$  decreases. The solid lines show that the inclusion of radiative transfer further decreases the temperature at which  $n_e = N^0$ . This occurs because the Lyman series photons (especially Ly $_{\alpha}$ ), emitted in the recombination process, can be absorbed by the neutrals in the volume, which can then be collisionally ionized before re-emitting the photon. This photon trapping decreases the effective recombination rate. It also greatly complicates both the experimental determination of the recombination rate and the modelling of the entire problem because the radiation transfer makes the problem both non-linear and non-local. As emphasized in Fig. 1, electron temperature is also an important quantity when determining rates. Finally, the electron density influences the recombination rate (both directly and through multi-step effects), and therefore must also be known or estimated.

#### 3.1 Establishment of “Recombinations Per Photon”

Knowledge of the local temperature, density, and opacity is, in principle, enough to determine the recombination rate by directly evaluating the recombination rate coefficient,  $\alpha_{eff}^{rec}$ . However, the recombination rate coefficient, in both the optically thick and optically thin

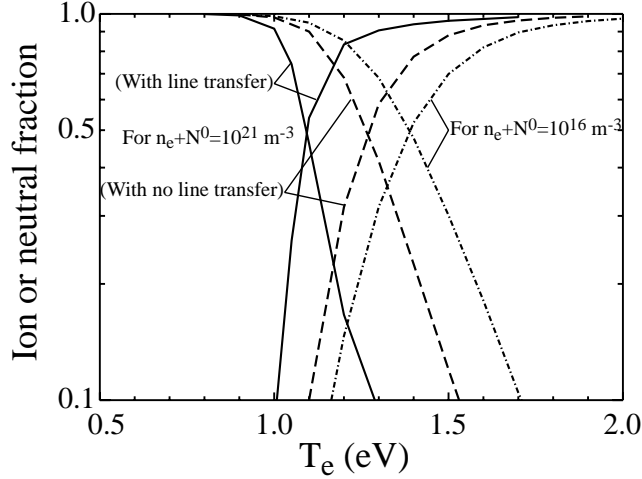


Figure 1: The three pairs of curves show the ion and neutral fraction vs  $T_e$  in the absence of particle transport. The monotonically decreasing (increasing) curves show the neutral (ion) fraction. The dot-dashed curves illustrate the low density case. The dashed curves show the balance at divertor-like densities, but excluding opacity effects. The solid curves show the same case including the effects of opacity.

limits, can be a strong function of temperature: evaluated at  $n_e \sim 10^{21} \text{ m}^{-3}$  and  $T_e$  in the 0.7-1.0 eV range,  $\frac{1}{\alpha} \frac{\partial \alpha}{\partial T_e}$  varies between  $\sim -5$  and  $-3 \text{ eV}^{-1}$ . Thus, precise evaluation of the recombination rate using the appropriate rate coefficient after measurement of the temperature and density requires an extremely accurate  $T_e$  measurement. Determination of the rate coefficient is made less sensitive to the accuracy of temperature measurements by measuring the photons which are involved in the recombination process. This is one of the advantages of the ‘recombinations per photon’ concept. Calculated curves giving the number of recombinations per  $D_\gamma$  photon ( $R_{D_\gamma}$ ) in a plasma of  $n_e = 10^{21} \text{ m}^{-3}$  are shown in Fig. 2. The  $D_\gamma$  line is chosen because it remains optically thin in all relevant conditions and is easily accessible spectroscopically. It is seen that for  $D_\gamma$ ,  $\frac{1}{R_{D_\gamma}} \frac{\partial R_{D_\gamma}}{\partial T_e} \sim -2.5$  to  $-1 \text{ eV}^{-1}$  over the same 0.7 - 1.0 eV range, indicating a  $T_e$  sensitivity which is weaker than that for the effective recombination rate coefficient,  $\alpha_{eff}^{rec}$ . It is through these recombination per photon curves that the spatially resolved measurements of the Balmer (or Lyman) line intensities can be related to the effective recombination rates.

Calculation of the recombination per photon curves involves: 1) the use of a collisional-radiative (CR) model for determination of the excited state population densities; and 2) a model for the radiative transfer of the  $D^0$  emission. In the optically thin case, the number

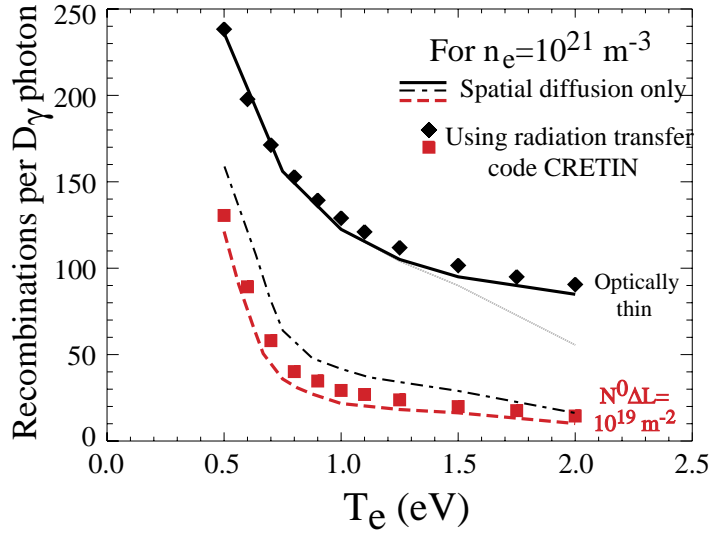


Figure 2: The number of effective recombinations per  $D_\gamma$  photon in an optically thin limit (solid line and diamonds), and for two cases in which  $\text{Ly}_{\alpha,\beta}$  are optically thick. The thick, dashed curve and the closed squares show the results for  $N^0\Delta L=1\times 10^{19} \text{ m}^{-2}$  using escape factor model and CRETIN, respectively. The thin, dot-dashed curve shows the case for  $N^0\Delta L=2\times 10^{18} \text{ m}^{-2}$ .

of recombinations per  $D_\gamma$  photon is:

$$R_{D_\gamma}(T_e, n_e, \tau(\lambda) = 0) = \frac{\alpha_{eff}^{rec} n_e n_i}{A_{5\rightarrow 2} n_5}, \quad (1)$$

where  $\tau(\lambda)$  indicates the optical depth at wavelength  $\lambda$ ,  $A_{5\rightarrow 2}$  is the transition probability, and  $n_5$  is the population density of the  $n=5$  level. This quantity is shown in Fig. 2 for  $n_e = 10^{21} \text{ m}^{-3}$  as the solid line. For this calculation, the CR model used was the Collisional Radiative Atomic and Molecular Data code (CRAMD) [5] which uses the semi-empirical rates from Ref. [9], modified to account for the effects of statistical plasma microfields [12], but does not include wavelength-diffusion effects. Results agree with those using the CR models of Johnson and Hinnov.[8] Although it is not shown in Fig. 2, there is a density dependence to the recombinations per photon curves. (There is a much stronger density dependence to the actual recombination rate.) Roughly the recombinations per photon scale as  $\sqrt{n_e}$ , i.e. if there are 2 recombinations per photon at  $n_e = 1 \times 10^{21} \text{ m}^{-3}$ , there are about 3 recombinations per photon at  $n_e = 2 \times 10^{21} \text{ m}^{-3}$ .

Curves giving the number of recombinations per photon have also been calculated using CRETIN. In order to compare results for the optically thin case, CRETIN was run under the condition that the neutral density times the characteristic size of the recombining region

along the line-of-sight ( $\Delta L$ ) was low and the trapping of the Lyman lines was negligible. This result is shown as the diamonds in Fig. 2. Since very similar CR rates were used in CRETIN, good agreement with the other results is expected and observed. However, the CRETIN result also shows that, in order for the plasma to be optically thin,  $N^0\Delta L$  must be  $< 10^{17} m^{-2}$ , a condition which is extremely unlikely in tokamak divertors (where  $\Delta L \sim 0.02 m$ ) if the measured temperatures are less than  $1.5 eV$ . Alternatively, very fast neutral transport would be required to keep  $N^0/n_e < 5 \times 10^{-3}$  at the  $0.5-1 eV$  temperatures measured in Alcator C-Mod. Thus, it is expected that opacity and radiative transfer play a significant role in the ionization balance in the divertor.

### 3.2 Opacity Significance

In the above section, determining the recombination rate was done in two ways: first by modelling photon diffusion in a uniform volume; and second, by modelling photon transport in both space and frequency using the CRETIN code. (In both cases  $T_i$  was taken to be equal to  $T_e$ . In the next section we discuss the implications of such a temperature assumption.) For the spatial-diffusion-only treatment, CRAMD was modified to include a model for photon transport through a cylinder of uniform temperature and density with a  $0.02 m$  diameter  $\Delta L$ . Using an escape factor formalism [13], the radiative transition probabilities were reduced by a factor of  $C/(1+C)$ , where  $C=0.33 \times (\lambda_{mfp}/\Delta L)^2$  and  $\lambda_{mfp}$  is the mean-free-path for photon absorption; this  $C$  depends on the product  $N^0\Delta L$ . In the cases where the Lyman lines are not optically thin, the definition for the number of recombinations per photon, Eq. 1, is modified to reflect the fact that the effective recombination rate is no longer a local quantity, i.e. :

$$R_{D_\gamma}(T_e, n_e, \tau(\lambda)) = \frac{\langle \alpha_{eff}^{rec} n_e n_i \rangle_{vol}}{E_{5 \rightarrow 2}}, \quad (2)$$

where  $\langle \rangle_{vol}$  is a volume average and  $E_{5 \rightarrow 2}$  is the average  $D_\gamma$  photon flux escaping the plasma volume. (Of course the Balmer lines are still thin in these cases.) The result is shown by the dashed curve in Fig. 2. As expected, the recombinations per photon drop rapidly as  $N^0\Delta L$  increases to  $\sim 2 \times 10^{18} m^{-2}$ . However, for larger values of  $N^0\Delta L$ , the recombinations per photon drop only slightly, since  $Ly_\alpha$  is strongly trapped in the interior of the volume. Thus the lower curves shown in Fig. 2 represent the appropriate ‘‘optically thick’’ limit for these plasmas.

The results using the spatial diffusion/escape factor modelling have been compared with those calculated using the CRETIN code. In this case the volume modelled was a  $0.02 m$  thick slab of uniform temperature and density. The results are shown in Fig. 2 where the

‘recombinations per photon’ curve calculated using CRETIN (the squares) is compared with the dashed curve. The CRETIN values are only slightly greater than those of the escape factor modelling. The conclusion reached using the two different models with two different (but simple) geometries is that the recombinations per photon are reduced from the optically thin values by a factor from  $\sim 2$  to 8, depending on  $T_e$ .

## 4 Alcator C-Mod MARFE Simulation in 1-D

Moving away from the toy problem presented in the previous section, we investigate an Alcator C-Mod midplane MARFE. Characterized by simple plasma parameter profiles and sharp gradients at the edges, this problem proved to be a stringent test for the code. Our results highlight the importance of including the Zeeman effect in reproducing experimental data in large magnetic field conditions.

Spectroscopic measurements estimate conditions inside the MARFE as  $T_e \sim 0.7$  eV and  $n_e \sim 2 - 3 \times 10^{21} \text{ m}^{-3}$ ; core plasma conditions are also well known. Gradients at the MARFE edge are sharp and profiles must match known core values; however the spatial behavior of the transition zone is not known. Thus profiles such as  $T_e$ ,  $n_e$  and neutral density were adjusted in an effort to fit measured  $\text{Ly}\beta$  to  $\text{Ly}\eta(8 \rightarrow 1)$  lines, the  $\text{D}\alpha$  line, and the Balmer and Lyman continua intensities. With so many free parameters and constraints, many combinations must be investigated to arrive at satisfactory results.

From simple ordering estimates, the importance of Zeeman splitting may be seen. Since this effect is not included in CRETIN, we estimated the properties of such an effect and adjusted with the profile parameters to approximate such behavior. CRETIN currently considers only three effects in the computation of the local line shape: the Doppler effect (both temperature-induced broadening and a drift-velocity induced shift) gives a shifted Gaussian profile; the natural line width; and a Stark Lorentzian half-width. Through convolution the three may be combined to yield a Voigt-shaped line profile. As detailed calculations show, the Zeeman effect is also of the same order as the Doppler and Stark effects — parametrically we know Doppler behaves as  $\frac{v_{th}}{c}$ , Stark like  $n_e^{\frac{2}{3}} r_b^2$ , and Zeeman like  $\frac{\omega_B}{\omega_o}$ . To give a specific example, for conditions suitable to the MARFE case under study, Zeeman splitting in the  $\text{Ly}\beta$  line is approximately 0.19B(T) meV. For a nominal 5.5 T magnetic field this gives 1.5 meV at the MARFE location. Similar estimates show the Stark line width of about 2.7 meV and a Doppler width of only 0.3 meV.

To emulate magnetic line broadening due to the Zeeman effect, it has been necessary to artificially enhance the ion temperature inside the MARFE region to several tens of electron volts so as to reach an equivalent breadth. The impact of this procedure can be seen in

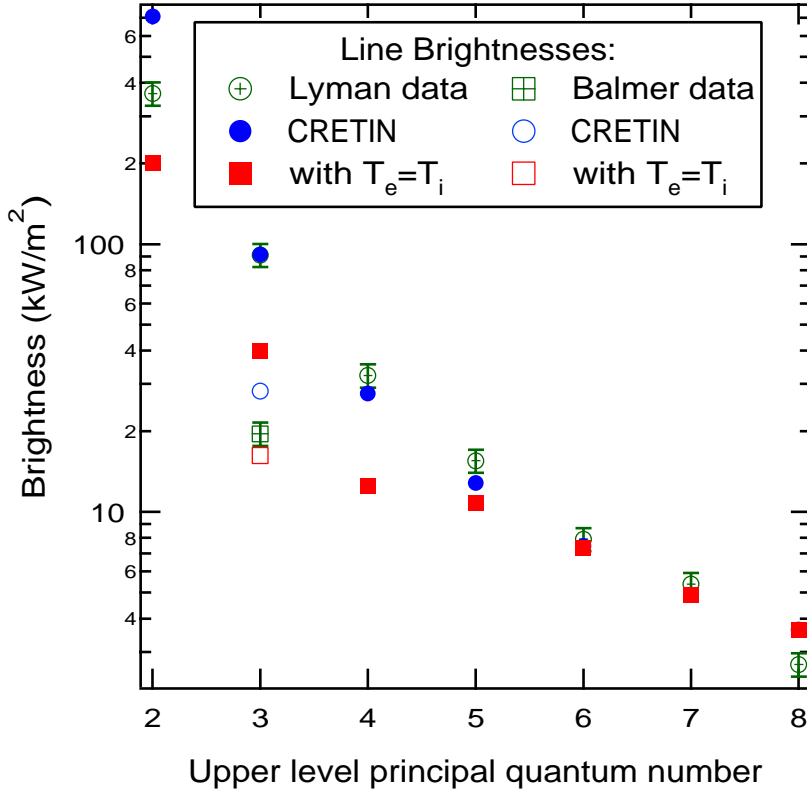


Figure 3: **Brightness of Lyman-series and  $D_\alpha$  lines from the 1-D MARFE model, comparing experimental measurement to two CRETIN runs, one with standard  $T_e$  and  $T_i$  profiles (noted  $T_e = T_i$ ) and one with enhanced ion temperature to reproduce the effect of Zeeman splitting.**

Fig. 3, where the normal case ( $T_e = T_i$ ) is shown next to the “enhanced” line width obtained by increasing  $T_i$ . However, this fix is also somewhat unsatisfactory since the effectiveness of magnetic line broadening as a wavelength scatterer is dependent on the Stark width. If the Stark width is much smaller than the Zeeman splitting (like for  $Ly_\alpha$  or the Balmer series) then the Zeeman components’ wings do not overlap and there is no significant wavelength diffusion. At the other extreme, for high- $n$  lines where the Stark width is very large, the magnetic broadening contribution is negligible (but so is the Doppler broadening). Hence, enhancing  $T_i$  is only effective when looking at lines where the increased Gaussian width is of the order of the Zeeman splitting, which happens, in our conditions, for the low-lying Lyman series lines starting at  $Ly_\beta$ . Therefore, through sacrificing the accuracy of a few input parameters we have been able to match the brightness of most the Lyman-series ( $Ly_\beta$  through  $Ly_\theta$ ) lines to within experimental accuracy.

## 5 Discussion

In the previous sections, several attempts to tweak CRETIN for comparison with experiment have been mentioned. Most notably is the emulation of the Zeeman effect which is necessary due to the presence of strong magnetic fields in tokamak plasmas. This section will suggest methods for evolving CRETIN to a state where it can handle magnetic fields and be unhindered by the current logical spatial mesh structure. We begin with some background information and the reader is referred to Mihalas[14] for more details; bound-bound transitions are then examined and an alternative absorption profile which may account for the Stark effect is suggested; magnetic line broadening may be treated by a similar approach; and finally, we recommend a technique for solving the radiation transfer equation on an arbitrary (non-logical) mesh.

### 5.1 Background: Radiation and Matter

As a reference for the next subsections, relevant equations are presented here in an extremely abbreviated form. For consistency, and to aid the unfamiliar reader, notation by Mihalas[14] has been used throughout this section with relevant pages placed within parenthesis.

Through definition of specific intensity  $I(\vec{r}, \vec{n}, \nu, t)$  (24) one may write the down the equation of radiation transfer in differential form as (35):

$$\mu \frac{\partial I_\nu}{\partial \tau_\nu} = I_\nu - S_\nu, \quad (3)$$

where  $d\tau(z, \nu) \equiv -\chi(z, \nu)dz$  (34),  $\mu \equiv \cos \theta$  where  $\theta$  is the angle between the direction of a photon ray and an arbitrarily oriented surface,  $S_\nu = \eta/\chi$  is the source function (35),  $\chi$  is the opacity (23) and  $\eta$  is the emissivity.

Of prominent importance in tokamak plasmas are bound-bound transitions, where one is looking at transitions between two states of an atom, denoted by  $i$  and  $j$  in the equations that follow. (Bound-free and free-free transitions are also important; since they are treated in similar to the bound-bound transitions they have been omitted for brevity.) Using the Einstein relations for bound-bound transitions (79):

$$A_{ji} \equiv \frac{2h\nu^3}{c^2} B_{ji} \quad (4)$$

$$g_i B_{ij} \equiv g_j B_{ji}, \quad (5)$$

one may appropriately define a line source function and a line absorption coefficient in Eq. 3 as (80):

$$\chi_l(\nu) = \left(\frac{n_i B_{ij} h \nu_{ij}}{4\pi}\right) \phi_\nu \left(1 - \frac{n_j B_{ji} \psi_\nu}{n_i B_{ij} \phi_\nu}\right) \quad (6)$$

$$S_l = \frac{n_j A_{ji} \psi_\nu}{n_i B_{ij} \phi_\nu - n_j B_{ji} \psi_\nu}, \quad (7)$$

where  $\phi_\nu$  is the normalized absorption coefficient (27) and  $\psi_\nu$  is an emission profile (28).

## 5.2 Natural-Doppler-Stark Broadening

CRETIN currently accounts for Doppler-natural-Stark broadening through construction of normalized absorption coefficients,  $\phi_\nu$  in Eq. 7. Through convolution of a Gaussian and Lorentzian profile [15], the resultant line profile is given by:

$$\phi_\nu = \frac{1}{G\sqrt{\pi}} H(a, x), \quad (8)$$

where  $H(a, x)$  is the Voigt function and  $a$  is the Voigt parameter given by:

$$H(a, x) = \frac{a}{\pi} \int_{-\infty}^{\infty} \frac{\exp -y^2}{(x-y)^2 + a^2} dy \quad (9)$$

$$a = \frac{\Gamma}{4\pi G} \quad (10)$$

$$\Gamma = \Gamma_{\text{Natural}} + 0.61\Gamma_{\text{Stark}} \quad (11)$$

$$G = \sqrt{(\Delta\nu_D)^2 + (3\Gamma_{\text{Stark}})^2} \quad (12)$$

$$\Delta\nu_D = \frac{\nu_o}{c} \sqrt{\frac{2kT}{m}}. \quad (13)$$

Ideally one would like to account for both the Stark and Zeeman effects through a similar formalism, however this is currently not possible. A method for including the Stark effect *via* a similar convolution treatment has been suggested by Biberman[16] and is included here merely as a potential remedy.

### 5.2.1 Quasi-Static Ion Approximation Method for Including the Stark Effect

If a quasi-neutral plasma is sufficiently dense, such that the number of particles within the Debye sphere is very large, a quasi-static ion approximation may be invoked. Under this approximation the influence of a neighboring electron on the radiating atom may be treated when calculating spectral line profiles — neglecting any external magnetic field — thereby accounting for the Stark effect. In this case the resultant line profile is given by:

$$\phi_\nu = \int_0^\infty \sum_{\alpha\alpha'} G_{\alpha\alpha'} P(F) \Psi_{\alpha\alpha'}(\nu, F) dF, \quad (14)$$

where  $F$  represents different values of the ion microfield,  $P(F)$  is the ion microfield distribution function,  $G_{\alpha\alpha'}$  is the fractional strength of the Stark component given by  $(n_i n_j m - n'_i n'_j m')$ ,  $\alpha = n_i n_j m$  are the quantum numbers and  $\Psi_{\alpha\alpha'}(\nu, F)$  is the profile of the individual Stark component. As defined by Biberman, for an ideal plasma these terms may be approximated as:

$$P(F) = \frac{P_H(x)}{F_o} \quad (15)$$

$$P_H(x) = \frac{2x}{\pi} \int_0^\infty \exp^{-y^{\frac{3}{2}}} y \sin(xy) dy \quad (16)$$

$$x = \frac{F}{F_o} \quad (17)$$

$$F_o = 2.6en_e^{\frac{2}{3}} \quad (18)$$

$$\Psi_{\alpha\alpha'}(\nu, F) = \frac{\gamma_{\alpha\alpha'}}{\pi} \frac{1}{(\nu - \nu'_{\alpha\alpha'} - \Delta\nu_{\alpha\alpha'}(F))^2 + \gamma_{\alpha\alpha'}^2} \quad (19)$$

$$\Delta\nu_{\alpha\alpha'}(F) = \frac{3}{2} [n'(2n'_i - n' + |m'| + 1) - n(2n_i - n + |m| + 1)] F \quad (20)$$

$$\gamma_{\alpha\alpha'} = \frac{32n_e}{3\langle v \rangle} \left[ \ln\left(\frac{r_{Debye}}{r_W}\right) + 0.215 \right] (1 + n^4) \quad (21)$$

$$\langle v \rangle = \sqrt{\frac{8T}{\pi m_e}} \quad (22)$$

$$r_W = \sqrt{\frac{2}{3}} \frac{\hbar n^2}{m_e \langle v \rangle}, \quad (23)$$

where  $P_H(x)$  is the Holtsmark distribution function,  $F_o$  is the Holtsmark field strength and  $r_W$  the Weisskopf radius. Although the above set of equations appears lengthy, they merely represent a simple approximation of the interaction of an electron within the Debye sphere of a radiating particle.

### 5.3 Magnetic Line Broadening

As has already been mentioned, the Zeeman splitting is of the same order as the Stark and Doppler widths. Ideally, the Zeeman effect will need to be treated by a successively more complex radiation-matter interaction model appropriate for tokamak conditions. For the Stark effect Biberman[16] looked at a very simple model which only accounted for the influence of electrons. The next step in such an evolution would be to look at the effects of

an external electric and magnetic field under the assumption that only two-body collisions are important.

## 5.4 Radiation Transfer Equation Solution

Note that the radiation transfer equation (Eq. 3) and Boltzmann equation with BGK collision operator are remarkably similar. Previous work in the area of neutral gas transport [17] has demonstrated the ability of an integral-operator technique to reformulate the kinetic equation in integral form; subsequent discretization then becomes trivial. Extending this work, which complements the method of solution currently used in CRETIN, it is possible to allow for a free grid and second order discretization schemes. As future work looks to couple CRETIN with plasma transport codes such as UEDGE [18], it might be necessary to treat complex boundaries (as radiation is non-local) and complicated non-rectangular connectivities (such as near the X-point ).[19] When such a case arises, one suggested remedy is to adapt the radiation transfer solution as necessary. In this subsection we verbally suggest how to evolve the current radiation transfer equation solution.

To transform the existing solution technique from a logical to a free grid we focus on the initial trajectory point. As any higher dimensional problem is always reduced to 1-D through the use of an appropriate operator, we can say that the final trajectory point value is computed from knowledge of the initial trajectory point. (An approximate ideal function is used at the final point — e.g., blackbody for photons and Maxwellian for neutrals — but this is unimportant in this discussion.) Previously, this initial trajectory was always taken along an edge connecting neighboring nodes, its distance from the final trajectory point was computed and other values which were estimated by weighing them according to their distance to the nodes on the edge. To allow for a grid-free solution we remove the dependence of the initial point on the edge. This is done by first *choosing* a distance between initial and final point and then looking for neighbors to compute initial point values — this will require increasing the number of nodes used in the weighing scheme above the logical grid’s two.

Second order accuracy has already been obtained in theory and is in the implementation phase. The discretization method chosen is a simple second degree Taylor polynomial and second order difference formulas (center for interior regions and backward for boundaries).

## Acknowledgements

The authors would like to thank A. Wan of LLNL for use of CRETIN and making this MIT-LLNL collaboration possible.

## References

- [1] H. Scott and R. Mayle. GLF — a simulation code for X-ray lasers. *Applied Physics B*, 58:35, 1994.
- [2] D.E. Post, R.V. Jensen, C.B. Tarter, W.H. Grasberger, and W.A. Lokke. Steady-state radiative cooling rates for low-density, high-temperature plasma. *At. Data Nucl. Data Tables*, 20:397, 1977.
- [3] Russell A. Hulse. Numerical studies of impurities in fusion plasmas. *Nuclear Technology/Fusion*, 3:259, March 1983.
- [4] D. Post, J. Abdallah, R.E.H. Clark, and N. Putvinskaya. Calculations of energy losses due to atomic processes in tokamaks with applications to the International Thermonuclear Experimental Reactor divertor. *The Physics of Plasmas*, 2(6):2328, June 1995.
- [5] A. Pigarov and S.I. Krasheninnikov. Application of the collisional-radiative, atomic-molecular model to the recombining divertor plasma. *Physics Letters A*, 222:251, 1996.
- [6] S.I. Krasheninnikov, A.Yu. Pigarov, and D.J. Sigmar. Plasma recombination and divertor detachment. *Physics Letters A*, 214:285, 1996.
- [7] J.L. Terry, B. Lipschultz, A.Yu. Pigarov, S.I. Krasheninnikov, B. LaBombard, D. Lumma, H. Ohkawa, D. Pappas, and M. Umansky. Volume recombination and opacity in Alcator C-Mod divertor plasmas. *Physics of Plasmas*, 5(5):1759, May 1998.
- [8] L.C. Johnson and E. Hinnov. Ionization, recombination, and population of excited levels in hydrogen plasmas. *Journal of Quantitative Spectroscopy and Radiative Transfer*, 13(4):333, April 1973.
- [9] L.C. Johnson. Approximations for collisional and radiative transition rates in atomic hydrogen. *Astrophysical Journal.*, 174(1):227, May 1972.
- [10] R.W. Lee. Fits for hydrogenic Stark-broadened line profiles for the elements carbon to argon. *Journal of Applied Physics.*, 58(1):612, July 1985.
- [11] H. Griem. *Spectral Line Broadening by Plasmas*. Academic Press, New York, 1974.
- [12] A.Yu. Pigarov, J. Terry, and B. Lipschultz. Study of the discrete-to-continuum transition in a Balmer spectrum from Alcator C-Mod divertor plasmas. To be published in *Plasma Phys. and Controlled Fusion.*, 1998.

- [13] V.V. Sobolev. *Soviet Astron. Astrophysics J.*, 1:678, 1957.
- [14] Dimitri Mihalas. *Stellar Atmospheres*. W.H. Greeman and Company, San Francisco, 2nd edition, 1978.
- [15] C.W. Allen. *Astrophysical Quantities*, pages 86–89. Atlantic Highlands, London, 3rd edition, 1976.
- [16] L.M. Biberman, L.G. D’Yachkov, and V.S. Vorob’ev. Integral and spectral line radiation from plane layer of nonequilibrium plasma (benchmark). Correspondence Date: September 1998.
- [17] M.L. Adams, S.I. Krasheninnikov, and O.V. Batishchev. Feasibility study of an iterative finite difference approach to kinetic modeling of neutral particles in edge plasmas. Technical Report PSFC/RR-97-7, Massachusetts Institute of Technology Plasma Fusion Center, April 1997.
- [18] D.A. Knoll, P.R. McHugh, S.I. Krasheninnikov, and D.J. Sigmar. Simulation of dense recombining divertor plasmas with a Navier-Stokes neutral transport model. *The Physics of Plasmas*, 3(1):293, 1996.
- [19] A.S. Wan, H.E. Dalhed, H.A. Scott, D.E. Post, and T.D. Rognlien. Detailed radiative transport modeling of a radiative divertor. *Journal of Nuclear Materials*, 220-222:1102, 1995.